J. Fluid Mech. (2023), *vol*. 960, A10, doi:10.1017/jfm.2023.185

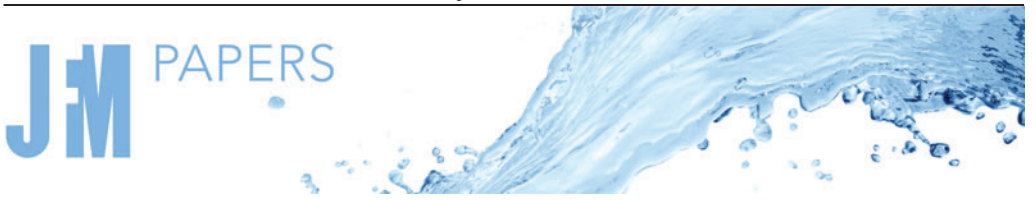

Effects of physical property changes of expelled respiratory liquid on atomization morphology

Biruk Teka Gidreta[1] **and Hyoungsoo Kim**[1],†

[1]Department of Mechanical Engineering, Korea Advanced Institute of Science and Technology (KAIST), 291 Daehak-ro, Yuseong-gu, Daejeon 34141, Republic of Korea

(Received 2 August 2022; revised 21 December 2022; accepted 28 February 2023)

A better understanding of the fluid dynamics of disease transmission by disintegrated respiratory droplets has been the focus of great attention since the recent outbreak of COVID-19. In particular, human respiratory activities such as coughing, sneezing and even talking and eating expel a large amount of pathogen-laden droplets. Particularly, during eating or drinking, the physical properties of saliva can be changed. In this study, we investigate the atomization morphology of expelled artificial saliva mixtures from the perspective of varying fluid physical properties, specifically surface tension and dynamic viscosity. Using high-speed shadowgraph experiments on artificial saliva, we visualize and analyse the disintegration of saliva liquid sheets into ligaments and droplets. We find that the viscosity and surface tension affect the droplet size formed from expelled saliva and follow scaling laws that have been previously observed and predicted for constant shear viscosity. We conclude that the changes in physical properties of saliva induced by eating and drinking tend to favour the formation of smaller droplets during sneezing or coughing, which could drive the airborne transmission pathway of pathogens. Furthermore, we derive a theoretical model based on scaling arguments that shows the breakup time of ligaments produced from the artificial saliva mixtures is dependent on the capillary number.

Key words: aerosols/atomization

1. Introduction

The fragmentation of a liquid sheet into droplets is a ubiquitous phenomenon found in nature and industry with several applications (Marmottant & Villermaux 2004; Villermaux 2007; Eggers & Villermaux 2008). The precise knowledge and control of the

† Email address for correspondence: hshk@kaist.ac.kr

droplet size formed from spray is important in many areas such as spray coating, inkjet printing and agriculture (Kooij *et al.* 2018). Understanding liquid sheet breakup is also important for the prevention and containment of airborne disease transmission, which has gained much attention after the outbreak of COVID-19. Soon after the World Health Organization declared COVID-19 a pandemic, evidence emerged showing the airborne transmission of the virus (Morawska & Cao 2020; Morawska & Milton 2020; Richard *et al.* 2020; Wilson, Corbett & Tovey 2020).

Airborne transmission of pathogens via expelled respiratory droplets is mainly carried out by small droplets. Wells (1934) compared the evaporation time and settling time of droplets ranging from 1 to 1000 μm and found that droplets of size greater than 100 μm settle faster than they evaporated. On the contrary, droplets with diameters less than 100 μm evaporate faster than they can settle to the ground and the droplet nuclei remain suspended in the air for a longer period of time. Wells' result served as a basis for the dichotomization of respiratory transmission modes depending on the droplet size. Small droplets laden with pathogens can travel several metres in the air and might play a significant role in the transmission of COVID-19 in indoor environments (Morawska & Cao 2020). Many studies have been conducted to understand the fluid dynamics of the breakup of expelled respiratory liquids (Scharfman *et al.* 2016; Poulain & Bourouiba 2019; Bourouiba 2020, 2021; Reyes *et al.* 2021). Sneezing, coughing (Bourouiba, Dehandschoewercker & Bush 2014) and even speech (Abkarian *et al.* 2020) produce a multiphase, turbulent gas cloud containing pathogen-laden droplets. The ejecta from sneezing and coughing include distinctively separated droplets as well as bags of fluid, which continue to fragment into droplets outside the mouth.

The fragmentation mechanism of a liquid is affected by its physical properties such as the surface tension and viscosity (Dombrowski & Fraser 1954). Food and beverages can change such physical properties of saliva. Saliva is a non-Newtonian fluid with shear-thinning behaviour, and thus, the viscosity of saliva could change due to shear rate changes in the mouth. For instance, a shear rate of 4 s^{-1} is associated with the movement of particles across the tongue, while shear rates of 160 and up to 500 s^{-1} correspond to speech and eating, respectively (Vissink *et al.* 1984; Gittings *et al.* 2015). Additionally, the physical presence of food in the mouth also affects the viscosity of saliva, whose composition and viscosity depends on the type of stimulus (Briedis, Moutrie & Balmer 1980). The viscosity of saliva at a shear rate of 4 s^{-1} is around 30 mPa s, and we take this as the pre-eating baseline viscosity value. This value decreases to around 1 mPa s due to the high shear stress induced by eating. Meanwhile, many foods and drinks contain surfactants, both natural and synthetic, that can lower the surface tension of saliva. Natural surfactants such as lecithin from egg yolk and synthetic surfactants such sorbitan esters are used in the preparation of many foods such as mayonnaise, dressings and deserts (Kralova & Sjöblom 2009). Furthermore, beverages that contain alcohol can also lower the surface tension of saliva. The surface tension of saliva could increase from the baseline value, around 67 to around 70 mN m^{-1} during eating due to the salinity of food. More importantly, the surface tension could decrease by more than half to 25 mN m^{-1} during consumption of an alcoholic drink. Eating could also induce changes in the viscoelasticity of saliva; acidic food has been shown to stimulate the secretion of saliva with an increased elasticity (Stokes & Davies 2007; Davies, Wantling & Stokes 2009).

In general, the atomization of complex fluids can be characterized using dimensionless numbers such as the capillary, Weber and Ohnesorge numbers (McKinley 2005). In this study, among the various physical properties, we focus on the effects of viscosity and surface tension, which can be changed significantly during eating or drinking, as opposed

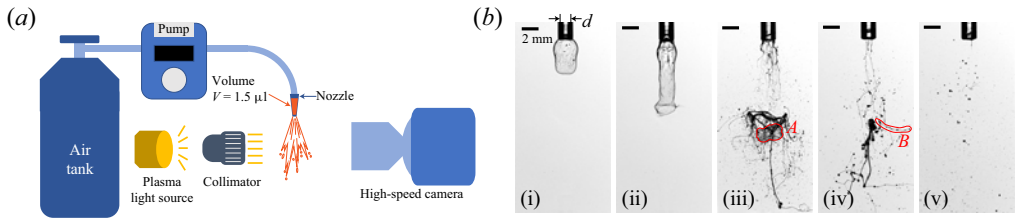

Figure 1. (*a*) Schematic of the experimental set-up. Air with a step-function pressure profile is applied on to a 1.5 µl liquid sample placed inside a nozzle of 1.1 mm internal diameter (*d*). (*b*) The breakup process of a liquid volume in response to applied pressure. (i)–(ii) The liquid column grows along the axial direction until it ruptures. (ii) The time it takes for the liquid column to rupture is defined as the breakup time, *t*. (iii) The liquid sheet then breaks down into fluid bags (A) and ligaments. (iv)–(v) The ligaments thin and stretch forming beads-on-a-string structures (B) before they finally fragment into droplets.

to, for instance, density, which remains relatively constant. The risk of airborne COVID-19 transmission posed by eating or drinking is especially high since, during dining, we take off our face masks, which are the most effective way of protecting ourselves from COVID-19 and other airborne diseases.

While many studies have been conducted to characterize the effect of physical properties of fluids on the atomization mechanism of Newtonian liquid jets, to our best knowledge, the effect of saliva fluid properties on its atomization morphology has rarely been studied. In this work, we experimentally study the atomization mechanism of artificial saliva mixtures from the perspective of varying physical properties. Our work has two main objectives; first, we attempt to visualize and analyse the atomization morphology of human saliva using high-speed shadowgraph experiments on artificial saliva. Second, we investigate the effect of the physical properties of saliva on its atomization mechanism. We use probability density functions of the droplet size and the Sauter mean diameters to characterize the effect of saliva fluid properties on the atomization of expelled saliva.

2. Experiment

2.1. *Experimental set-up*

In this study, we performed high-speed shadowgraph experiments on the atomization of artificial saliva. A schematic of the experimental set-up is shown in figure 1(*a*). An artificial saliva sample of 1.5 µl volume was placed inside a cylindrical nozzle of 1.1 mm internal diameter (*d*), onto which a step-function profile pressure was applied for 100 ms by a pressure controller (Fluigent FLOW EZ, France). Air was supplied to the nozzle by a high-pressure air tank with pressure values ranging from 0.1 to 4 bar. The atomization morphology was recorded with a high-speed camera (Photron fastcam SA-Z, Japan), and a high-power plasma light source (HPLS343, Thorlabs, Inc., USA) was used to illuminate the background and create a bright field. The collimator placed between the light source and the object helps create a uniform light distribution. The breakup process was recorded at frame rates ranging from 20 000 to 70 000 frames-per-second with an exposure time of 1/1 680 000 or 1/2 880 000 s.

2.2. *Materials*

For our experiments, we selected two artificial saliva products that had similar physical properties to natural saliva after rheological and surface tension measurements; first, artificial saliva for dental and medical research (1700-0305, Pickering Laboratories Inc.,

Liquid sample	Surface tension (mN m^{-1})	Viscosity at a shear rate of 1000 s^{-1} (mPa s)
A	66.7 ± 0.4	25
A + 0.05 CMC SDS	45.0 ± 0.6	25
A + 0.8 CMC SDS	31.5 ± 0.1	25
A + 10 wt % ethanol + 10 wt % glycerol	47.3 ± 0.3	25
A + 40 wt % ethanol + 40 wt % glycerol	28.1 ± 0.3	25
B	72.4 ± 0.6	1
B + 5 wt % ethanol	55.6 ± 1.5	1
B + 18 wt % ethanol	41.2 ± 0.5	1
B + 45 wt % ethanol	28.6 ± 0.2	1
B + 0.04 CMC SDS	55.0 ± 0.8	1
B + 1.0 CMC SDS	38.0 ± 0.4	1
B + 35 wt % glycerol	58.4 ± 0.5	2.5
B + 50 wt % glycerol	56.5 ± 0.3	5
B + 62 wt % glycerol	52.5 ± 0.4	10
B + 70 wt % glycerol	52.1 ± 0.5	20
B + 80 wt % glycerol	51.2 ± 0.7	40

Table 1. The composition and physical properties of the liquid samples investigated; A and B are artificial saliva products for dental and medical research and pharmaceutical research, respectively.

USA), which we labelled as 'saliva A', is formulated with sodium carboxymethyl cellulose to increase the viscosity and make it behave like natural human saliva. The second artificial saliva sample, labelled as 'saliva B', is artificial saliva for pharmaceutical research (1700-0304, Pickering Laboratories Inc., USA) and is formulated for drug dissolution. The viscosity measurements were conducted using a Modular Compact Rheometer MCR 502 (Anton Paar GmbH, Austria). Measurements were carried out at 37 °C with the shear rate increasing logarithmically from 1 to 1000 s^{-1}. The viscosity values of the liquid samples at a shear rate of 1000 s^{-1}, which represents the shear rate during sneezing or coughing (Zahm *et al.* 1991; Lai *et al.* 2009; Vasquez *et al.* 2014), are given in table 1. The surface tension measurements were conducted using the pendant drop method. The shape of the drop hanging from a needle is determined from the balance of forces which include the surface tension of the liquid being investigated. Images of the drop hanging were captured and the surface tension was calculated using an in-house MATLAB processing (Stauffer 1965).

Furthermore, we altered the physical properties of the artificial saliva samples. To change the viscosity, we used glycerol ($\geqslant$99.0 % purity, Sigma-Aldrich, USA), which alters the viscosity without significantly affecting the surface tension of the liquid. We used ethanol ($\geqslant$99.5 % purity, Sigma-Aldrich, USA) and SDS (sodium dodecyl sulphate, $\geqslant$98.0 % purity, Sigma-Aldrich, USA) to change the surface tension of saliva B and a combination of ethanol and glycerol to change the surface tension of saliva A. The compositions as well as the viscosity at a shear rate of 1000 s^{-1} and surface tension values of the fluid samples used are shown in table 1.

3. Results and discussion

3.1. *Breakup morphology of expelled respiratory liquid*

Using the experimental set-up described in § 2.1, we observed the evolution of the breakdown of an expelled saliva through a nozzle. As can be seen in figure 1(*b*), after

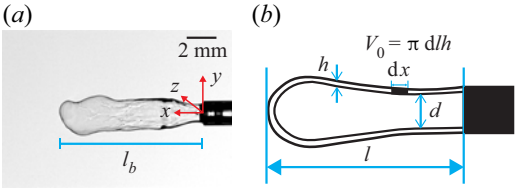

Figure 2. (*a*) The formation and growth of transverse waves at the interface between the liquid sheet and the surrounding air where l_b is the breakup critical length. (*b*) Variable notations for the sheet thickness (h) and column length (l) where $V_0 = \pi\, \mathrm{d}lh$.

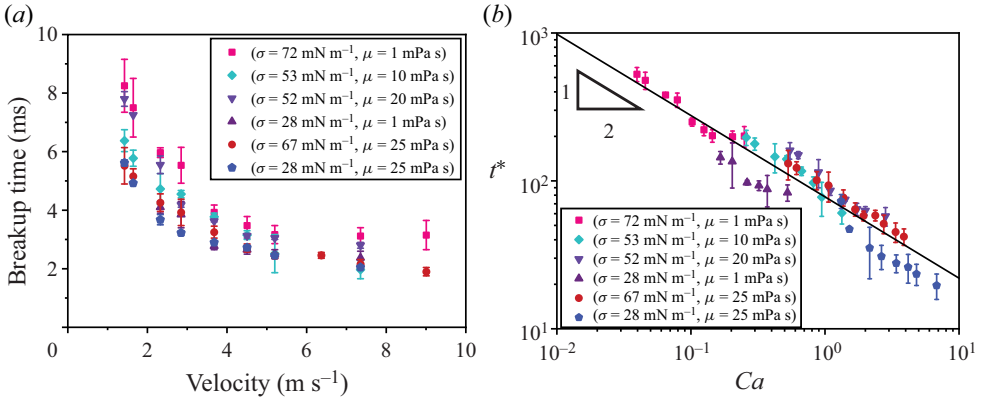

Figure 3. (*a*) The breakup time t (as defined in (ii) of figure 1*b*) against the velocity U of the airflow. (*b*) Theoretical model for liquid column breakup (3.7) where $t^* = t/[\mu/\sigma(V_o/2N_1\pi d)^{1/2}]$ and $Ca = \mu U/\sigma$.

the liquid emerges from the nozzle, it grows along the nozzle direction and continues to thin as a hollow shell, during which transverse waves form at the interface between the liquid and the surrounding air. These waves grow and destabilize the liquid sheet, leading to its breakdown. The liquid sheet then disintegrates into liquid bags and ligaments (see (iii) of figure 1*b*). As shown in (iv) and (v) of figure 1(*b*), the liquid bags burst to form ligaments, which form beads-on-a-string structures and eventually fragment into droplets (see also supplementary movie 1 available at https://doi.org/10.1017/jfm.2023.185).

We performed experiments by altering the pressure of the airflow and observed that the breakup time and length of the growing liquid column depend on the pressure. Here, the breakup time is defined as the time elapsed from the impingement of airflow to the burst of the liquid sheet. We defined the breakup length as the maximum length the liquid column grows to before rupturing, as shown in figure 2(*a*). As the velocity increases, the breakup time decreases, while the breakup length increases. The jet velocity (U) was measured using 10 µm hollow glass spheres and showed a quadratic relation with the pressure (p), i.e. $p \propto U^2$. The breakup times of various liquids are presented in figure 3(*a*). We found that the dimensionless breakup time ($t^* = t/[\mu/\sigma(V_o/2N_1\pi d)^{1/2}]$), where σ is the surface tension and μ is the dynamic viscosity of the liquid, shows a power-law dependence on the capillary number ($Ca = \mu U/\sigma$) with a slope of $-1/2$ (see figure 3*b*). Here, N_1 is defined as $(2 - N)/N$ where N is a constant value to consider the viscous effect (Dombrowski & Johns 1963).

3.2. *Theoretical modelling*

To understand our experimental findings, we performed theoretical modelling based on works by Squire (1953) and Dombrowski & Johns (1963), which showed that the breakup of liquid sheets occurs through the formation of transverse waves which grow until the sheet breaks down (see figure 2). Considering a sheet that is thinning with time and moving in the x-direction with velocity U through stationary gas, the equation of motion of the sheet mid-way between the two gas/liquid interfaces is obtained by inter-relating the forces acting on the liquid sheet. Here, the displacement of the neutral axis of sheet from undisturbed position is in the y-direction, as sketched in figure 2(a). These forces are caused by gas pressure, liquid surface tension, inertia and viscosity. Assuming perturbations only in the y-direction, these four forces per unit length can be scaled as: (i) pressure force: $F_p = 2n\rho_g U^2 \pi \,\mathrm{d}y$, (ii) surface tension force: $F_\sigma = 2\sigma\pi d(\partial^2 y/\partial x^2)$, (iii) inertial force: $F_i = \rho_l(h(\partial^2 y/\partial t^2) + (\partial h/\partial t)(\partial y/\partial t))\pi d$ and (iv) viscous force: $F_\mu = \mu(\partial^3 y/\partial t \partial x^2)\pi \,\mathrm{d}h$, where ρ_g: density of air ($\approx$1.225 kg m^{-3}), d: the inner diameter of the nozzle (1.1 mm), σ: surface tension ($\approx$28–72 mN m^{-1}), ρ_l: density of the liquid ($\approx$1000 kg m^{-3}), h: thickness of the liquid sheet [O(0.1 mm)], μ: viscosity ($\approx$1–40 mPa s), y: the displacement of neutral axis of sheet from undisturbed position in the y-direction and n: wavenumber for viscous liquids (Dombrowski & Johns 1963).

Hence the total force on a finite length dx is

$$2n\rho_g U^2 \pi \,\mathrm{d}y \,\mathrm{d}x + 2\sigma\pi d\frac{\partial^2 y}{\partial x^2}\mathrm{d}x + \rho_l \pi d\left(h\frac{\partial^2 y}{\partial t^2} + \frac{\partial h}{\partial t}\frac{\partial y}{\partial t}\right)\mathrm{d}x + \mu\pi d\frac{\partial^3 y}{\partial t \partial x^2}h\,\mathrm{d}x \simeq 0. \tag{3.1}$$

Using order of magnitude estimates, we find that $F_p \sim O(10^{-3})$ N, $F_\sigma \sim O(10^{-3})$ N, $F_i \sim O(10^{-5})$ N and $F_\mu \sim O(10^{-3})$ N. Thus, we assume a balance of the pressure and surface tension forces with the viscous force

$$2n\rho_g U^2 \pi \,\mathrm{d}y \,\mathrm{d}x + 2\sigma\pi d\frac{\partial^2 y}{\partial x^2}\mathrm{d}x + \mu\pi d\frac{\partial^3 y}{\partial t \partial x^2}h\,\mathrm{d}x \sim 0. \tag{3.2}$$

For a sinusoidal wave motion, $y = T\sin(nx + \varepsilon)$ where n is wavenumber and ε is phase angle, (3.2) yields

$$2n\rho_g U^2 \pi d[T\sin(nx+\varepsilon)]\,\mathrm{d}x - 2\sigma\pi n^2 d[T\sin(nx+\varepsilon)]\,\mathrm{d}x \sim \mu\pi\,\mathrm{d}n^2\frac{\partial[T\sin(nx+\varepsilon)]}{\partial t}h\,\mathrm{d}x, \tag{3.3}$$

which can be simplified by substituting for h in terms of the initial volume $V_o = \pi\,\mathrm{d}hl$ and taking $l = Ut$ to find

$$2\rho_g U^2 - 2n\sigma \sim \frac{\mu V_o}{\pi\,\mathrm{d}U}n\frac{1}{t^2}. \tag{3.4}$$

The wavenumber of the dominant wave for a viscous liquid is given as $n = N\rho_g U^2/2\sigma$, where N is a constant that accounts for the viscous effects (Dombrowski & Johns 1963).

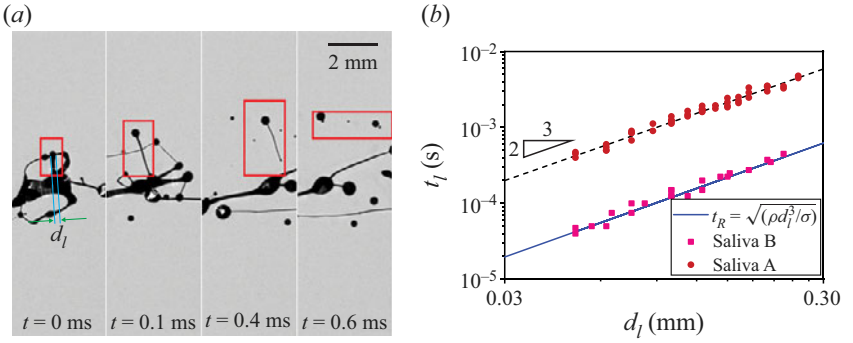

Figure 4. (*a*) The fragmentation process of a ligament of saliva A into droplets. (*b*) The breakup time (t_l) of ligaments of salivas A and B for various initial ligament diameters (d_l).

Introducing this equation into our relationship, we find

$$N_1 \rho_g U^2 \sim \frac{\mu V_o \rho_g U}{2\pi\, \mathrm{d}\sigma} \frac{1}{t^2}, \tag{3.5}$$

where $N_1 = (2 - N)/N$. Rearranging the relationship and using the capillary number, $Ca = \mu U/\sigma$,

$$t \sim \frac{\mu}{\sigma} \left(\frac{V_o}{N_1 2\pi d} \right)^{1/2} Ca^{-1/2}. \tag{3.6}$$

Defining $t^* = t/[\mu/\sigma\,(V_o/2N_1\pi d)^{1/2}]$, we find an expression relating the dimensionless breakup time to the capillary number

$$t^* \sim Ca^{-1/2}. \tag{3.7}$$

The expression in (3.7) explains our experimental observations. The dimensionless breakup time is plotted against the capillary number in figure 3(*b*). Taking N_1 to be proportional to μ, we find that the measurement data of the various liquids investigated collapse into a single curve.

3.3. *Droplet formation*

The fragmentation of ligaments into droplets is driven by surface tension, which gives rise to the Rayleigh–Plateau (RP) instability, as shown in figure 4(*a*). Low-viscosity Newtonian ligaments breakdown via the RP instability on the capillary time scale, $t_R = \sqrt{\rho d^3/\sigma}$. Figure 4(*b*) shows the ligament breakup times of salivas A and B at 1 bar (a shear rate of $\sim$1000 s^{-1}), which corresponds to the shear rate during sneezing or coughing. The low-viscosity, non-viscoelastic saliva B ligaments breakup on the capillary time scale. However, ligaments of saliva A fragment on a time scale approximately an order of magnitude higher than that predicted by the RP instability. Our experiments show that the beads-on-a-string structures on the ligaments retard the ligament breakup. Beads-on-a-string structures arise when the inertial, capillary, viscous and elastic forces are balanced (Clasen *et al.* 2006; Bhat *et al.* 2010). The formation of beads-on-a-string structures indicates the presence of viscoelastic effects. These structures play a critical role in retarding droplet formation and thus affect the droplet size distribution. Our experiments also show that, prior to the final separation of droplets, the 'beads' on the structures merge after the 'string' has thinned down.

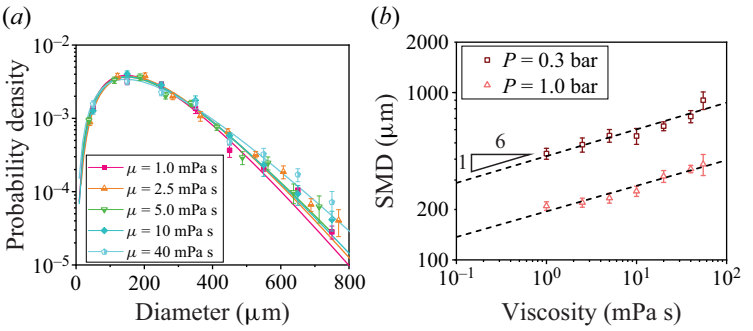

Figure 5. (*a*) The droplet size distribution of fluids of varying viscosities at 1 bar. (*b*) The effect of viscosity on the Sauter mean diameter (SMD) for two different pressure inputs.

3.4. *Effect of saliva physical properties on its atomization mechanism*

3.4.1. *Effect of viscosity*

First of all, we investigated the effect of dynamic viscosity on the atomization of respiratory fluids. As the viscosity increases, the pinch off time of the ligaments increases. This in turn delays the eventual breakup of the ligaments by delaying the breakup time. We characterized the effect of viscosity on the droplet size using the droplet size distribution and Sauter mean diameter plots. To investigate the effect of viscosity on the atomization mechanism of liquid sheets, we varied the viscosity by as much as a factor of 40, from 1 mPa s for pure saliva B to 40 mPa s for a mixture of saliva B with 80 wt % glycerol. This range covers the reported viscosity values of saliva at different shear rates (Gittings *et al.* 2015). We measured the probability density function of the droplet size using image processing by an in-house MATLAB program on high-speed images, and the experimental data are fitted with a gamma distribution, which is known to represent the droplet size distribution, including the fragmentation of viscoelastic liquids (Villermaux 2007; Keshavarz *et al.* 2016). Our experiments also show that the gamma distribution fits the experimental data more closely than other distributions such as log-normal or Poisson distributions. As can be seen in figure 5(*a*), the droplet size distribution is very weakly correlated with the viscosity, only showing a noticeable difference for the highest-viscosity liquid. Figure 5(*b*) shows the relationship between the viscosity and the Sauter mean diameter (SMD, D32); SMD is defined as the diameter of a droplet that has the same volume to surface area ratio as that of the entire spray and can be expressed as the ratio of the third to the second moment of the probability density function (Pacek, Man & Nienow 1998; Kowalczuk & Drzymala 2016).

$$\frac{\displaystyle\int_{d_{min}}^{d_{max}} d^3 q(d)\,\mathrm{d}d}{\displaystyle\int_{d_{min}}^{d_{max}} d^2 q(d)\,\mathrm{d}d}, \tag{3.8}$$

where d_{min} and d_{max} represent, respectively, the minimum and maximum values of diameter of the histogram $q(d)$. Alternatively, in terms of a finite number of discrete size classes,

$$D_{32} = \frac{\sum_{i=1}^{n} N_i D_i^3}{\sum_{i=1}^{n} N_i D_i^2}, \tag{3.9}$$

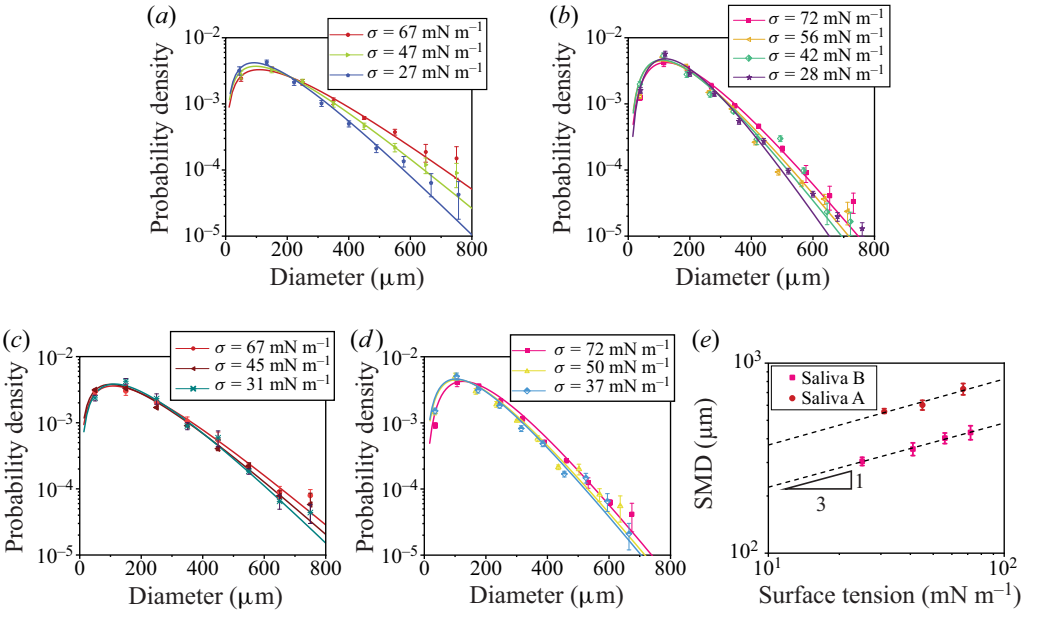

Figure 6. The effect of surface tension on the droplet size at 1 bar. The droplet size distribution of (*a*) ethanol–saliva A, (*b*) ethanol–saliva B, (*c*) SDS–saliva A and (*d*) SDS–saliva B mixtures. (*e*) The effect of surface tension on the SMD.

where N_i and D_i are the number of droplets and mean diameter of a class, respectively. The SMD is widely used to characterize the drop size in sprays, and it is especially important in calculations where the active surface area is important (Lefebvre & McDonell 2017).

Our experiments show that the SMD increases as the viscosity increases. Considering the changes in the shear rate in the mouth, the viscosity of saliva could decrease from 4 mPa s at low shear rates ($\sim$100 s^{-1}) to 1 mPa s at high shear rates ($\sim$1000 s^{-1}). Keeping other parameters constant, this represents $SMD_2/SMD_1 = (\mu_2/\mu_1)^{1/6} = (1/4)^{1/6} = 0.79$. Thus, the mean diameter of saliva could decrease by up to 21 % due to the change in viscosity induced by eating or drinking.

3.4.2. *Effect of surface tension*

We changed the surface tension of the liquids in two ways, using ethanol and surfactants (SDS). To characterize our experimental observations, we investigated the droplet size distributions and mean drop diameters of the liquids. Figure 6 shows the droplet size distribution and SMD measurements conducted at 1 bar. As can be seen in figures 6(*a*) and 6(*b*), when the surface tension decreases, smaller droplets are formed. The droplet size distributions of both ethanol–saliva A and ethanol–saliva B mixtures show that lowering the surface tension results in the formation of smaller droplets. Although the ethanol–saliva mixtures show clearly the effect of surface tension on the droplet size, surfactant–saliva mixtures do not alter the size distribution as significantly (see figure 6*c*,*d*). For the surfactants case, the time scale of the breakup of the liquid sheets could be retarded compared with the ethanol–saliva mixture. Because, in the surfactant thin film, immediately after a surface of the thin film is stretched, the surface tension could be comparable to that of pure saliva liquid; the equilibrium value is only reached

after a certain time, which depends on the diffusion rate and the adsorption rate of the surfactant (Gildnyi, Stergiopoulos & Wolfram 1976).

The effect of surface tension on the droplet size is further characterized using the SMD, as shown in figure 6(*e*). The SMD results show a power-law dependence on the surface tension. Our experiments show that the surface tension of saliva could decrease from around 72 to 27 mN m^{-1} during eating or drinking. Keeping other parameters constant, this represents $\mathrm{SMD}_2/\mathrm{SMD}_1 = (\sigma_2/\sigma_1)^{1/3} = 0.72$. Thus, the mean diameter of saliva could decrease by up to 28 % due to the change in surface tension induced by eating or drinking. This observation has important implications; much of the food we eat consists of surfactants, both natural and synthetic, that can lower the surface tension in the mouth during eating, and alcoholic beverages also can lower the surface tension of saliva due to their ethanol content. Therefore, food can lower the surface tension of saliva, which leads to the formation of smaller droplets from expelled liquids during eating.

3.4.3. *Theoretical background*

The disintegration of a viscous liquid sheet into unstable ligaments, which eventually break down into droplets, has been thoroughly discussed by Dombrowski & Johns (1963). They found an expression for the diameter of the ligament d_L (cm) in terms of the operating conditions

$$d_L = 0.9614\left[\frac{k^2\sigma^2}{\rho_a\rho_L U^2}\right]^{1/6}\left[1 + 2.6\mu_L\left(\frac{k\rho_a^4 U^8}{72\rho_L^2\sigma^5}\right)^{1/3}\right]^{1/5}, \tag{3.10}$$

where σ (mN m^{-1}) is the liquid surface tension, μ_L (mPa s) is the liquid viscosity, ρ_a (g cm^{-3}) is the density of the surrounding medium, ρ_L (g cm^{-3}) is the density of the liquid, U (cm s^{-1}) is the velocity of the radiating sheet and k is a constant obtained by choosing a hyperbolic relationship between the sheet thickness h and the time t; i.e. $ht = k$.

The relation between the drop size and wavenumber, assuming the waves grow until their amplitude equals the ligament radius, is given by

$$D_{32}^3 = \frac{2\pi d_L^2}{n}. \tag{3.11}$$

Combining (3.10) and (3.11) results in

$$D_{32} = 1.88 d_L[1 + 3Oh]^{1/6}, \tag{3.12}$$

where $Oh = \mu_L/(\rho_L\sigma d_L)^{1/2}$ is the Ohnesorge number. For the liquids in our study, $Oh \ll 1$, giving

$$D_{32} \simeq 1.88 d_L \sim \sigma^{1/3} \tag{3.13}$$

which explains our experimental observations of SMD dependency on the surface tension. Dombrowski & Johns (1963) compared (3.12) with experimental data and a subsequent empirical equation developed by Hasson & Mizrahi (1961) given by

$$D_{32} = 0.071\left[\frac{k^2\sigma^2}{\rho_L U^2}\right]^{1/6}\mu^{1/6}, \tag{3.14}$$

and found that the two equations (3.12) and (3.14) compare favourably with each other in the experimental range of 3 mPa s $< \mu_L <$ 25 mPa s, which is similar to the viscosity range in our experiment.

4. Conclusion

In this work, we studied the atomization morphology of mixtures containing artificial saliva in which the surface tension and dynamic viscosity were varied. Using high-speed shadowgraph experiments, we visualized the evolution of the breakdown of artificial saliva mixtures. We observed that the breakup time decreases and the breakup length increases as the velocity of the impinging airflow increases. Using scaling arguments based on the forces acting on the growing liquid column, we derived a theoretical model that explicates our experimental observations. Furthermore, we found that the fragmentation time of saliva filaments is approximately an order of magnitude higher than that of low-viscosity Newtonian fluids. We also estimated that the mean diameter of the artificial saliva mixtures can decrease by up to 21 % due to viscosity changes and by up to 28 % due to surface tension changes. Although the precise effect of different foods on the physical properties of saliva is complex, we expect that in general the physical property changes of saliva brought about by eating and drinking would decrease the mean droplet size during sneezing or coughing events by up to 43 %. Smaller droplets derive the airborne transmission pathway of pathogens since they remain suspended for a longer time and can travel a larger distance than do larger droplets. Therefore, we conclude that eating and drinking change the physical properties of saliva in a way that likely facilitates the airborne transmission of pathogens via expelled respiratory droplets, although it is unclear how long the effects would last after swallowing. Thus, in addition to the other physiological and hydrodynamic factors discussed in other studies, the effect of eating and drinking should also be carefully considered to minimize airborne disease transmission.

Supplementary movie. Supplementary movie is available at https://doi.org/10.1017/jfm.2023.185.

Funding. This work was supported by the 'Development of indoor airflow control and air purification technology' project through the National Research Council of Science & Technology (NST), funded by the Ministry of Science (CPS-21-02-KICT) in South Korea. Also, this work was partially supported by the Basic Science Research Program through the National Research Foundation (NRF) of Korea funded by the Korean Government (MSIT: 2021R1A2C2007835).

Declaration of interests. The authors report no conflict of interest.

Author ORCIDs.
Biruk Teka Gidreta https://orcid.org/0000-0002-4107-7413;
Hyoungsoo Kim https://orcid.org/0000-0002-2393-723X.

References

Abkarian, M., Mendez, S., Xue, N., Yang, F. & Stone, H.A. 2020 Speech can produce jet-like transport relevant to asymptomatic spreading of virus. *Proc. Natl Acad. Sci. USA* **117** (41), 25237–25245.

Bhat, P.P., Appathurai, S., Harris, M.T., Pasquali, M., McKinley, G.H. & Basaran, O.A. 2010 Formation of beads-on-a-string structures during break-up of viscoelastic filaments. *Nat. Phys.* **6** (8), 625–631.

Bourouiba, L. 2020 Turbulent gas clouds and respiratory pathogen emissions: potential implications for reducing transmission of COVID-19. *J. Am. Med. Assoc.* **323** (18), 1837–1838.

Bourouiba, L. 2021 The fluid dynamics of disease transmission. *Annu. Rev. Fluid Mech.* **53**, 473–508.

Bourouiba, L., Dehandschoewercker, E. & Bush, J.W.M. 2014 Violent expiratory events: on coughing and sneezing. *J. Fluid Mech.* **745**, 537–563.

Briedis, D., Moutrie, M.F. & Balmer, R.T. 1980 A study of the shear viscosity of human whole saliva. *Rheol. Acta* **19** (3), 365–374.

Clasen, C., Eggers, J., Fontelos, M.A., Li, J. & McKinley, G.H. 2006 The beads-on-string structure of viscoelastic threads. *J. Fluid Mech.* **556**, 283–308.

Davies, G.A., Wantling, E. & Stokes, J.R. 2009 The influence of beverages on the stimulation and viscoelasticity of saliva: relationship to mouthfeel? *Food Hydrocolloid.* **23** (8), 2261–2269.

DOMBROWSKI, N. & FRASER, R.P. 1954 A photographic investigation into the disintegration of liquid sheets. *Phil. Trans. R. Soc. Lond.* A **247** (924), 101–130.

DOMBROWSKI, N. & JOHNS, W.R. 1963 The aerodynamic instability and disintegration of viscous liquid sheets. *Chem. Engng Sci.* **18** (3), 203–214.

EGGERS, J. & VILLERMAUX, E. 2008 Physics of liquid jets. *Rep. Prog. Phys.* **71** (3), 036601.

GILDNYI, T., STERGIOPOULOS, C. & WOLFRAM, E. 1976 Equilibrium surface tension of aqueous surfactant solutions. *Colloid Polym. Sci.* **254** (11), 1018–1023.

GITTINGS, S., TURNBULL, N., HENRY, B., ROBERTS, C.J. & GERSHKOVICH, P. 2015 Characterisation of human saliva as a platform for oral dissolution medium development. *Eur. J. Pharm. Biopharm.* **91**, 16–24.

HASSON, D. & MIZRAHI, J. 1961 The drop size of fan spray nozzles. *Trans. Inst. Chem. Engrs* **39**, 415–422.

KESHAVARZ, B., HOUZE, E.C., MOORE, J.R., KOERNER, M.R. & MCKINLEY, G.H. 2016 Ligament mediated fragmentation of viscoelastic liquids. *Phys. Rev. Lett.* **117** (15), 154502.

KOOIJ, S., SIJS, R., DENN, M.M., VILLERMAUX, E. & BONN, D. 2018 What determines the drop size in sprays? *Phys. Rev.* X **8** (3), 031019.

KOWALCZUK, P.B. & DRZYMALA, J. 2016 Physical meaning of the sauter mean diameter of spherical particulate matter. *Particul. Sci. Technol.* **34** (6), 645–647.

KRALOVA, I. & SJÖBLOM, J. 2009 Surfactants used in food industry: a review. *J. Dispers. Sci. Technol.* **30** (9), 1363–1383.

LAI, S.K., WANG, Y.-Y., WIRTZ, D. & HANES, J. 2009 Micro- and macrorheology of mucus. *Adv. Drug Deliv. Rev.* **61** (2), 86–100.

LEFEBVRE, A.H. & MCDONELL, V.G. 2017 *Atomization and Sprays*. CRC Press.

MARMOTTANT, P. & VILLERMAUX, E. 2004 On spray formation. *J. Fluid Mech.* **498**, 73–111.

MCKINLEY, G.H. 2005 Dimensionless groups for understanding free surface flows of complex fluids. *SOR Rheol. Bull.* **72**, 6–9.

MORAWSKA, L. & CAO, J. 2020 Airborne transmission of SARS-CoV-2: the world should face the reality. *Environ. Intl* **139**, 105730.

MORAWSKA, L. & MILTON, D.K. 2020 It is time to address airborne transmission of coronavirus disease 2019 (COVID-19). *Clin. Infect. Dis.* **71** (9), 2311–2313.

PACEK, A.W., MAN, C.C. & NIENOW, A.W. 1998 On the Sauter mean diameter and size distributions in turbulent liquid/liquid dispersions in a stirred vessel. *Chem. Engng Sci.* **53** (11), 2005–2011.

POULAIN, S. & BOUROUIBA, L. 2019 Disease transmission via drops and bubbles. *Phys. Today* **72** (5), 70.

REYES, J., FONTES, D., BAZZI, A., OTERO, M., AHMED, K. & KINZEL, M. 2021 Effect of saliva fluid properties on pathogen transmissibility. *Sci. Rep.* **11** (1), 1–14.

RICHARD, M., *et al.* 2020 SARS-CoV-2 is transmitted via contact and via the air between ferrets. *Nat. Commun.* **11** (1), 1–6.

SCHARFMAN, B.E., TECHET, A.H., BUSH, J.W.M. & BOUROUIBA, L. 2016 Visualization of sneeze ejecta: steps of fluid fragmentation leading to respiratory droplets. *Exp. Fluids* **57** (2), 1–9.

SQUIRE, H.B. 1953 Investigation of the instability of a moving liquid film. *Brit. J. Appl. Phys.* **4** (6), 167.

STAUFFER, C.E. 1965 The measurement of surface tension by the pendant drop technique. *J. Phys. Chem.* **69** (6), 1933–1938.

STOKES, J.R. & DAVIES, G.A. 2007 Viscoelasticity of human whole saliva collected after acid and mechanical stimulation. *Biorheology* **44** (3), 141–160.

VASQUEZ, E.S., BOWSER, J., SWIDERSKI, C., WALTERS, K.B. & KUNDU, S. 2014 Rheological characterization of mammalian lung mucus. *RSC Adv.* **4** (66), 34780–34783.

VILLERMAUX, E. 2007 Fragmentation. *Annu. Rev. Fluid Mech.* **39**, 419–446.

VISSINK, A., WATERMAN, H.A., GRAVENMADE, E.J.S., PANDERS, A.K. & VERMEY, A. 1984 Rheological properties of saliva substitutes containing mucin, carboxymethylcellulose or polyethylenoxide. *J. Oral. Pathol. Med.* **13** (1), 22–28.

WELLS, W.F. 1934 On air-borne infection: study II. Droplets and droplet nuclei. *Am. J. Epidemiol.* **20** (3), 611–618.

WILSON, N., CORBETT, S. & TOVEY, E. 2020 Airborne transmission of COVID-19. *Br. Med. J.* **370**, m3206.

ZAHM, J.M., KING, M., DUVIVIER, C., PIERROT, D., GIROD, S. & PUCHELLE, E. 1991 Role of simulated repetitive coughing in mucus clearance. *Eur. Respir. J.* **4** (3), 311–315.